JOURNAL OF SOLID STATE CHEMISTRY 64, 22–29 (1986)

Investigation of the Crystal Chemical and Ferroelectric Properties in the Vicinity of $LiNbO_3$ and $LiTaO_3$ inside the Ternary Systems Li_2O–Nb_2O_5–$(TiO_2)_2$ and Li_2O–Ta_2O_5–$(SnO_2)_2$

BRAHIM ELOUADI[1] AND MOHAMMED ZRIOUIL

Applied Solid State Chemistry Laboratory, Faculty of Sciences, Charia Ibn Batota Rabat, Morocco

Received August 5, 1985; in revised form October 14, 1985

A crystal chemical study has been carried out for the ternary systems Li_2O–M_2O_5–$(M'O_2)_2$ (M = Nb, M' = Ti; M = Ta, M' = Sn), in order to characterize and delimit the extension of domains of solid solutions in the vicinity of $LiNbO_3$ and $LiTaO_3$. The nature of the nonstoichiometry within these regions of solid solution has been found to be of a cationic excess or deficit. No evidence for anionic deficit has been found in this study. The ferroelectric Curie temperature T_C decreases as the composition deviates from $LiNbO_3$ or $LiTaO_3$. The decline in T_C has been interpreted on the basis of the electrostatic interactions resulting from either cationic excess or deficit. © 1986 Academic Press, Inc.

1. Introduction

In previous studies we investigated the effect of tetravalent cations M'^{4+} (M' = Ti; Zr) on crystal chemical and ferroelectric properties of $LiTaO_3$ (*1–6*). An interpretation of the change of ferroelectric Curie temperature vs composition has been put forward in the case of solid solutions with cationic excess and evidence for tetrahedrally coordinated Li^+ clusters in $Li_{1+5x}Ta_{1-x}O_3$ ($0 \leqq x \leqq 0.07$) and $Li_{1+y}Ta_{1-y}O_3$ ($y < 0.1$) has been given by the ^7Li NMR technique (*5*). The present study of the ternary systems Li_2O–Nb_2O_5–$(TiO_2)_2$ and Li_2O–Ta_2O_5–$(SnO_2)_2$ has been carried out in order to get more insight into the relationship between changes in structure and ferroelectric properties due to tetravalent cations. The tin system presents a big advantage, since the Sn^{4+} environment can be studied either by NMR or Mössbauer spectroscopy techniques.

Furthermore, Ti-doped $LiNbO_3$ is a very important material for optical wave guides, and although considerable efforts have been devoted to study TiO_2 diffusion into $LiNbO_3$ single crystals, little research has been conducted to lead to an understanding of the crystal chemical driving forces of this interaction: stoichiometry, phase equilibrium, etc. (*7–15*). As reported by various authors, the technique used for the fabrication of these devices is TiO_2 diffusion into $LiNbO_3$. In addition to the fact that $LiNbO_3$ single crystals may be nonstoichiometric, Ti^{4+} cations cannot be introduced into bulk $LiNbO_3$ without changing its composition, lattice constants, etc.; as a matter of fact, the chemical reaction involved during this

[1] To whom all correspondence should be addressed: Visiting Professor for 1 year at the Physics Department, Oklahoma State University, Stillwater, Okla. 74078.

0022-4596/86 $3.00

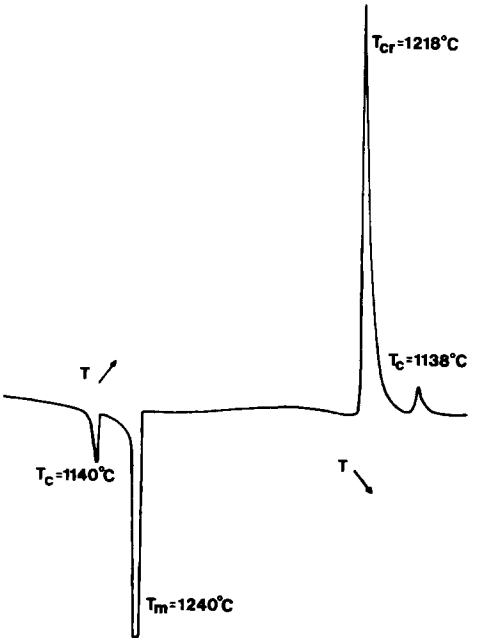

FIG. 1. Typical DTA curve obtained for the composition $Li_{1.035}Nb_{0.965}Ti_{0.035}O_3$. T_C, ferroelectric Curie temperature; T_m, melting temperature; T_{cr}, crystallization temperature.

diffusion should be considered as a solid state reaction of the ternary system Li_2O–Nb_2O_5–TiO_2. Therefore, deeper knowledge of the physicochemical properties of the system (in the vicinity of $LiNbO_3$) seems to be necessary in order to have a better control in the manufacture of wave guides.

2. Experimental Procedure

2.1. Samples Preparation

Powder samples were synthesized by standard solid state techniques, using high-purity Li_2CO_3, Nb_2O_5, Ta_2O_5, TiO_2, and SnO_2. The desired compositions were prepared from the appropriate mixture of starting materials. Several 12-hr heat treatments, interspersed with grinding, were necessary in order to obtain a pure single phase. The firing temperatures varied between 600 and 1100°C for the niobium system, and from 600 to 1350°C for that with tantalum. Observation of weight loss (before and after heat treatment) and X-ray analysis were used for checking of purity and structural characterization of the synthesized materials.

2.2. Ferroelectric Curie Temperature Measurements

In the system Li_2O–Ta_2O_5–$(SnO_2)_2$, thermal variation of the dielectric constant has been used to determine the ferroelectric Curie temperature (T_C) at the peak of $\varepsilon_r'(T)$ curve. Dielectric measurements were performed at 1 kHz with a Hewlett–Packard (4262A) capacitance bridge. Heating and cooling rates of 0.25 to 1°C/min were used. For the Li_2O–Nb_2O_5–(TiO_2) system, μ-DTA technique is more appropriate than the dielectric one, because the particularly high values of T_C are accompanied by a drastic increase in the dielectric loss which did not allow accurate balance of the capacitance bridge. Figure 1 gives a typical DTA curve obtained for the composition $Li_{1.035}Nb_{0.965}Ti_{0.035}O_3$.

3. Results and Discussion

3.1. Stoichiometry and Crystal Chemical Analysis

Figures 2a and b show the extension of the solid solutions investigated for the two ternary systems, Li_2O–Nb_2O_5–$(TiO_2)_2$ and Li_2O–Ta_2O_5–$(SnO_2)_2$. Nonstoichiometry inside the two ternary diagrams has been followed by density measurements in the same manner as already described in Refs. (*2, 6*). Plots of the density variation are given in Figs. 3 and 4. Results obtained from these experiments have allowed us to confirm that the change in nonstoichiometry (as shown in the diagrams of Figs. 2a and b) is identical to the one already observed in other systems, e.g., Li_2O–M_2O_5–$(M'O_2)_2$ (M = Nb, Ta; M' = Ti, Zr) (*3*). As

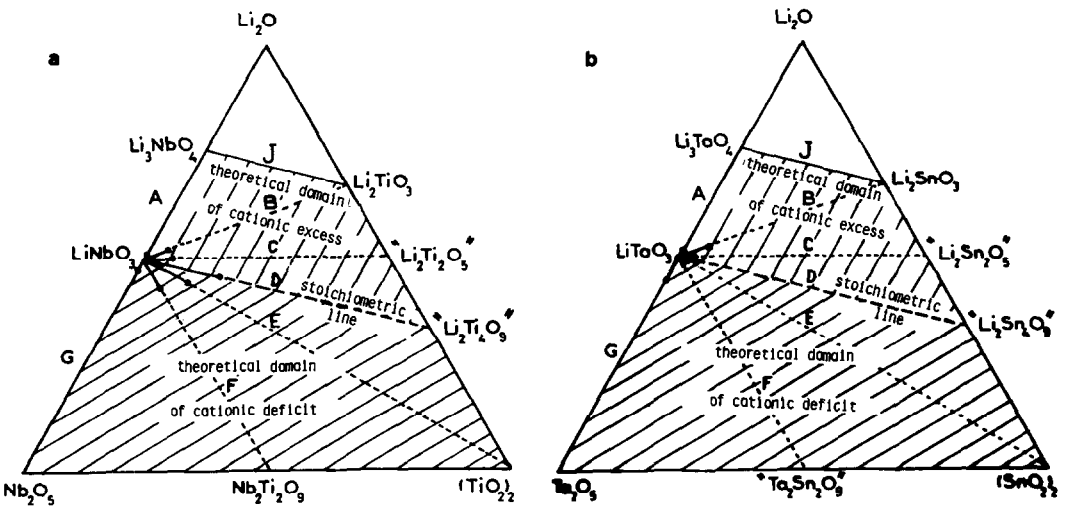

FIG. 2. Domain extension (–●) of the solid solutions investigated inside the ternary systems Li_2O–M_2O_5–$(M'O_2)_2$: (a) M = Nb, M' = Ti; (b) M = Ta, M' = Sn.

previously observed, within the error limits of our experimental procedure, the oxygen network is not affected by the nonstoichiometry which appears in these solid solutions (nonstoichiometry due to cationic excess or deficit) as shown in Table I. Therefore, a measure of deviation from stoichiometry, γ, can be defined as the difference between the number of cations per unit formula (in Table I) existing in each solid solution and the number of cations observed in stoichiometric $LiTaO_3$, for which $\gamma = 0$.

The limits of the solid solutions investigated have been determined by the appearance of impurity diffraction lines in the X-

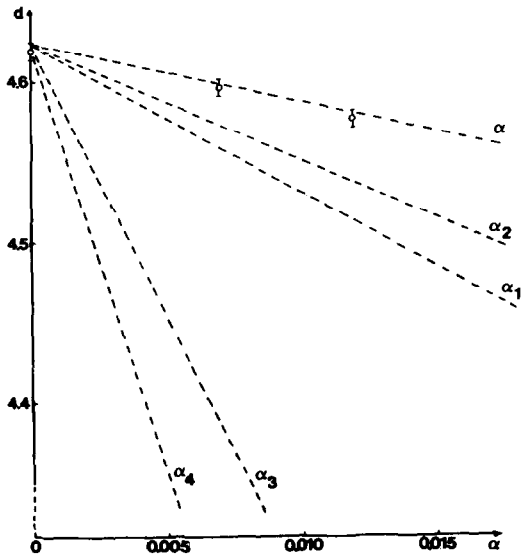

FIG. 3. Typical density variation curves obtained along the line F ($LiNbO_3$–"$Nb_2Ti_2O_9$") in the system Li_2O–Nb_2O_5–$(TiO_2)_2$. (○) Experimental values; (---) theoretical values.

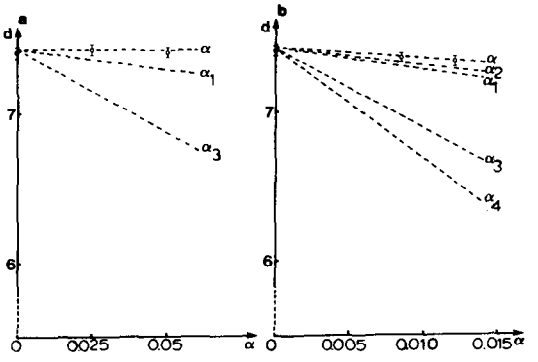

FIG. 4. Typical density variation curves obtained in the system Li_2O–Ta_2O_5–$(SnO_2)_2$, along: (a) the line F ($LiTaO_3$–"$Ta_2Sn_2O_9$"); (b) the line C ($LiTaO_3$–"$Li_2Sn_2O_5$"). (○) Experimental values; (---) theoretical values.

TABLE I

RECAPITULATION OF THE CRYSTAL CHEMICAL RESULTS OBTAINED FOR THE SYSTEMS Li_2O–M_2O_5–$(M'O_2)_2$ (M = Nb, M' = Ti; M = Ta, M' = Sn)

Region of the diagram	Line	Solid solution formula	γ: Stoichiometry deviation	Upper limit of x		Upper limit of γ		Ferroelectric Curie temperature (°C) of the solid solution limit	
				M = Nb M' = Ti	M = Ta M' = Sn	M = Nb M' = Ti	M = Ta M' = Sn	M = Nb M' = Ti	M = Ta M' = Sn
Cationic excess $\gamma > 0$	A	$Li_{1+x}M_{1-(x/5)}O_3$	$+\frac{4x}{5}$	0.05	0.07	0.04	0.056	1160	640
	B	$Li_{1+x}M_{1-x}M'_xO_3$	$+x$	0.06	0.08	0.06	0.08	1130	485
	C	$Li_{1+x}M_{1-5x}M'_{6x}O_3$	$+2x$	0.014	0.0085	0.28	0.017	1135	598
Stoichiometry $\gamma = 0$	D	$Li_{1-x}M_{1-3x}M'_{4x}O_3$	0	0.075	0.01	0	0	1140	600
Cationic deficit $\gamma < 0$	E	$Li_{1-x}M_{1-x}M'_{3x/2}O_3$	$-\frac{x}{2}$	0.125	0.03	−0.0625	−0.015	1020	590
	F	$Li_{1-x}M_{1-(x/3)}M'_{2x/3}O_3$	$-\frac{2x}{3}$	0.14	0.04	−0.093	−0.026	1165	620
	G	$Li_{1-x}M_{1+(x/5)}O_3$	$-\frac{4x}{5}$	0.085	0.12	−0.068	−0.096	1140	480

ray patterns of the sample. Trigonal space group $R3c$ (hexagonal indexing) has been used for the interpretation of the X-ray powder patterns. Due to the narrow regions of the solid solutions and the similarity of ionic radii for Li^+ (r = 0.68 Å); Nb^{5+} (r = 0.69 Å); Ta^{5+} (r = 0.68 Å); Ti^{4+} (r = 0.68 Å); and Sn^{4+} (r = 0.71 Å), one does not expect a big change in the unit cell parameters (*8*). This assumption is plainly confirmed by the experimental results collected in Figs. 5 and 6. Moreover, the introduction of titanium into either $LiNbO_3$ or $LiTaO_3$ lowers their melting temperatures thus facilitating crystal growth. In the case of line B (system Li_2O–Ta_2O_5–$(TiO_2)_2$), for example, the melting point is decreased from 1650°C for $LiTaO_3$, to 1460°C for the composition $Li_{1.14}Ta_{0.86}Ti_{0.14}O_3$ (*2*); along the solid solution D (system Li_2O–Nb_2O_5–$(TiO_2)_2$), the melting point is brought down from 1260°C for $LiNbO_3$ to 1186°C for the composition $Li_{0.925}Nb_{0.775}Ti_{0.3}O_3$ (Table II). The melting points (T_M) and crystallization temperatures (T_{cr}) of some compositions are listed in Table II. Comparison between the known ternary systems, Li_2O–M_2O_5–$(M'O_2)_2$ (M = Nb, Ta; M' = Ti, Zr, Sn), suggests the following crystal chemical remarks (*1–3*).

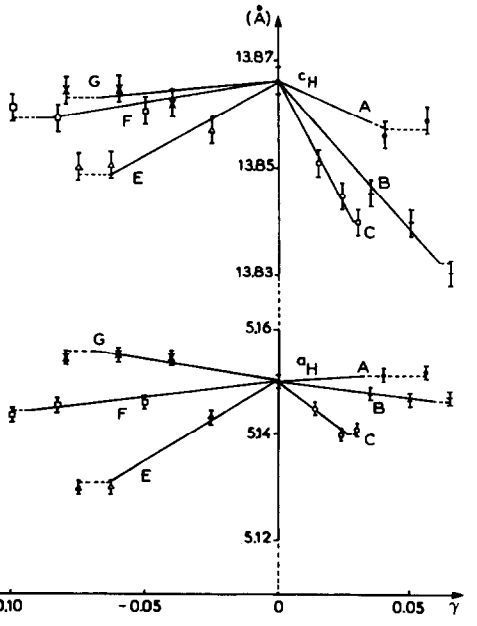

FIG. 5. Variation of lattice parameters versus γ along the solid solutions studied in the ternary diagram Li_2O–Nb_2O_5–$(TiO_2)_2$.

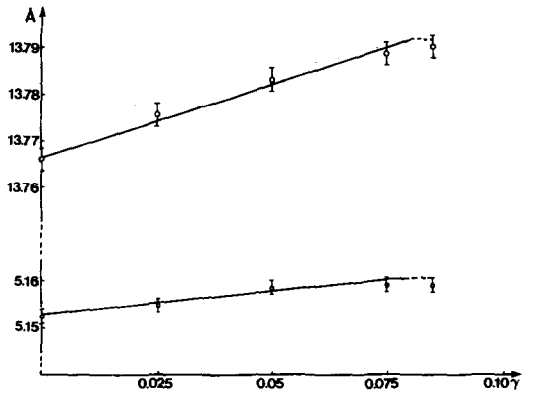

FIG. 6. Variation of the lattice parameters versus γ along the solid solution $Li_{1+x}Ta_{1-x}Sn_xO_3$.

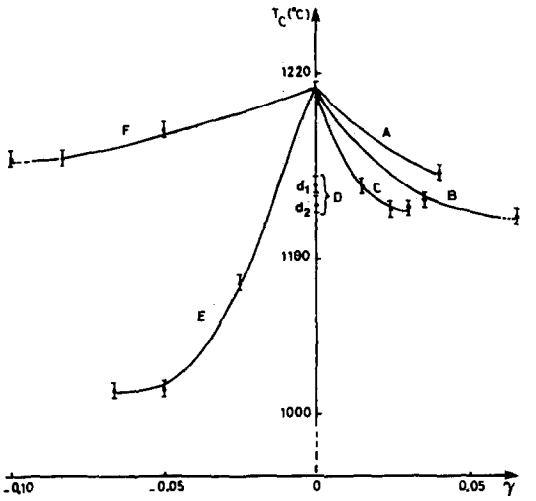

FIG. 7. Variation of the Curie temperature vs γ in the system Li_2O–Nb_2O_5–$(TiO_2)_2$.

—The width of the solid solution domain is always greater for the system involving Ta_2O_5, and is maximal inside the diagram Li_2O–Ta_2O_5–$(TiO_2)_2$.

—Therefore, the $LiTaO_3$ lattice seems to be more appropriate for cationic substitution than that of $LiNbO_3$.

—The $LiTaO_3$ network appears then as a more rigid ("stable") construction, with a greater ability to withstand the deformations resulting from nonstoichiometry without collapse.

3.2. *Dielectric Study*

$LiNbO_3$ and $LiTaO_3$ are two members of the oxide family having pronounced ferroelectric properties: $LiNbO_3$ has the highest known ferroelectric Curie temperature T_C = 1210°C, and among all the ferroelectric tantalates, $LiTaO_3$ has the highest value of T_C = 665°C (*17*). The origin of the ferroelectricity in these displacive ferroelectrics has been explained by Abrahams and Keve, to be due to cooperative cationic displacement inside the oxygen octahedra, along [001] of the hexagonal unit cell (*18*). In the paraelectric phase, these authors have

TABLE II

MELTING POINTS AND CRYSTALLIZATION TEMPERATURES OF THE SOLID SOLUTION LIMITS IN THE TERNARY DIAGRAM Li_2O–Nb_2O_5–$(TiO_2)_2$

Line	Formula	Upper limit of x	Melting point of the solid solution limit	Crystallization temperature (°C) of the solid solution limit
A	$Li_{1+x}Nb_{1-(x/5)}O_3$	0.05	1212	1209
B	$Li_{1+x}Nb_{1-x}Ti_xO_3$	0.06	1210	1206
C	$Li_{1+x}Nb_{1-5x}Ti_{6x}O_3$	0.014	1205	1203
D	$Li_{1-x}Nb_{1-3x}Ti_{4x}O_3$	0.075	1186	1186
E	$Li_{1-x}Nb_{1-x}Ti_{(3/2)x}O_3$	0.125	1197	1193
F	$Li_{1-x}Nb_{1-(x/3)}Ti_{(2/3)x}O_3$	0.14	1217	1210
G	$Li_{1-x}Nb_{1+(x/5)}O_3$	0.085	1234	1229

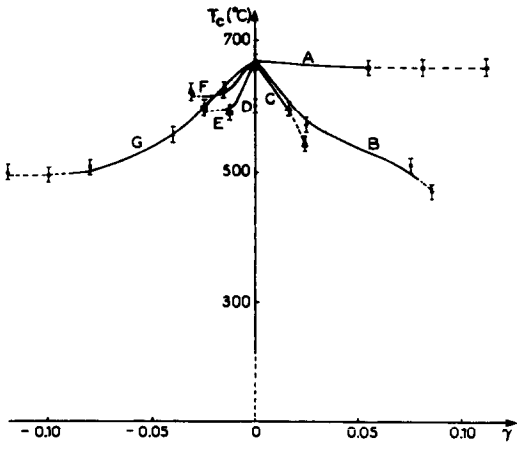

FIG. 8. Variation of the ferroelectric Curie temperature vs γ in the diagram Li_2O–Ta_2O_5–$(SnO_2)_2$.

shown that M^{5+} (M = Nb, Ta) is situated in the center of (MO_6) octahedra, while Li^+ is located in the center of a face common to two adjacent octahedra. The resulting space group for the prototype phase is $R\bar{3}c$.

The variation of Curie temperature versus the deviation from stoichiometry (γ) for the solid solutions reported in this paper is given in Figs. 7 and 8. In all cases, ferroelectric T_C decreases as the composition deviates from $LiNbO_3$ and $LiTaO_3$. The decline in T_C is, however, much more pronounced around the regions of cationic excess in the systems of Figs. 7 and 8, than in those previously published: Li_2O–Ta_2O_5–$(MO_2)_2$ (M = Ti, Zr) (*2, 4*). The crystal chemical origin of the drop in T_C along the lines A ($LiTaO_3$–Li_2O) and B ($LiTaO_3$–Li_2TiO_3) has already been clarified (*5*).

The explanation of the decrease in T_C for the other lines in Figs. 7 and 8 should be sought also in the structural modification of $LiNbO_3$ and $LiTaO_3$ lattices to suitably accommodate all of the cations existing in the corresponding solid solution formula (Table I). In order to interpret the drop in T_C vs γ, two regions in the ternary diagrams should be distinguished.

(*a*) *Cationic deficit region.* Therefore, let us consider Fig. 9, which shows the cationic distribution in stoichiometric and off-stoichiometric regions of the ternary diagrams. Noting the important role played by Li^+ displacement in the generation of spontaneous polarization ($\mathbf{P}_S$) it appears then, that their contribution to the total $\mathbf{P}_S$ is lessened with their deficiency: when one Li^+ cation is taken out of the lattice, simultaneously the corresponding dipole moments should be canceled ($\mathbf{P}_s = \Sigma_{i=1}^{N} \mathbf{u}_i = \Sigma_{i=1}^{N} q_i \mathbf{r}_i$; for Li vacancies we have: $q_{(Li^+)} = 0$, and the corresponding $\mu_{(Li^+)} = 0$). Consequently, the creation of Li^+ lacunae contributes to the decrease of the lattice spontaneous polarization. For example, if we consider the creation of two Li^+ (Li_1 and Li_2 in Fig. 9b) vacancies which are unfilled since we are considering the cationic deficit region, then the repulsive forces previously existing between Li_1 and M_1, and Li_2 and M_3 (M = Nb or Ta; Ti or Sn) will be removed. This cancellation will give rise to strong attractive electrostatic forces between cation M_1 and three adjacent oxygen

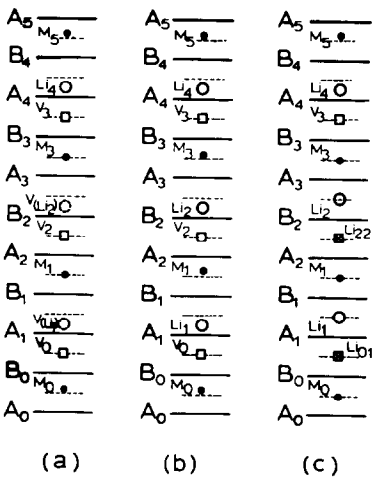

FIG. 9. Probable cationic distribution in the ferroelectric phase: (a) in the case of cationic deficit, (b) in stoichiometric $LiMO_3$ (M = Nb, Ta), (c) in the case of cationic excess.

anion layers (B_1, A_1, and B_0), and between M_3 and three adjoining oxygen layers $A_3B_2A_2$. The expected outcome of these interactions is the recall of M_1 and M_3 to the center of their octahedral sites, which results again in a decreasing of both $\mathbf{P}_S$ and the noncentrosymmetry character of the lattice (since $\mathbf{P}_S \rightarrow \mathbf{0}$). According to the previous arguments, the cationic vacancies should substantially contribute to making the network more centrosymmetric, as the deviation from stoichiometry (γ) increases. This tendency toward a centrosymmetrical lattice, in proportion to the value of γ; suggests that the rise in temperature necessary to overcome the ferroelectric (noncentrosymmetrical state) deformation should decrease when γ increases, and accordingly T_C should drop as observed in Figs. 7 and 8.

(*b*) *Region of cationic excess.* The smooth decrease of T_C vs γ along the line A ($LiTaO_3$–Li_2O) in the system Li_2O–Ta_2O_5–$(SnO_2)_2$, was shown in a former study wherein to be due to the existence of Li^+ ions in tetrahedrally coordinated clusters, which is qualitatively consistent with a value of T_C that is relatively independent of composition (*5*). Along the other lines, B and C for the system Li_2O–Ta_2O_5–$(SnO_2)_2$, the sharp decrease of T_C can be explained as follows:

—The unit cell contains more cations than in $LiMO_3$ (M = Nb, Ta) according to the formulae in Table I.

—These cations are all contained within a unit cell volume which is nearly the same as that of $LiMO_3$, because lattice parameters change only slightly over the whole range of the solid solutions studied.

—The repulsive forces resulting from the cationic excess should decrease the cooperative ferroelectric displacement existing in pure $LiMO_3$ (Fig. 9b): consider, for example (Fig. 9c), an excess of two Li^+ (Li_{01} and Li_{22}) placed in the vacancies V_0 and V_2; they repel strongly the neighboring cations, M_0, Li_1, M_1, Li_2, and M_3. The consequence of these repulsions will be that these cations will be forced back to the center of their octahedral sites where they should generate a very small, if not a null, contribution to the total spontaneous polarization ($\mathbf{P}_S$) of the lattice.

—There is, here again, the creation of a cluster (where $\mathbf{P}_S = \mathbf{0}$) which is perfectly integrated in the lattice structure. Thus the number of these clusters should increase as γ increases, and consequently the resulting network should proceed toward a more centrosymmetric state, which is consistent with T_C decreasing vs γ as observed in Figs. 7 and 8.

The drop in T_C between lines A, B, and C could be interpreted in a similar manner. Therefore, let us consider the compositions corresponding to $\gamma = 0.05$, in these three solid solutions. Their formulas can be deduced from Table I and written as follows:

$Li_{1.0625}M_{0.9875}O_3$ (A); $Li_{1.05}M_{0.95}M'_{0.05}O_3$ (B);

and

$Li_{1.025}M_{0.875}M'_{0.15}O_3$ (C);
(M = Nb, M' = Ti; M = Ta, M' = Sn).

As one moves from line A to line B and to C, the total number of highly charged cations (M^{+5} and M'^{4+}) per unit formula is increasing, whereas the number of Li^+ is diminishing. This is equivalent to an overcrowding of the nearly same volume by the same number of cations (γ constant) having individual charges which increase upon passing from line A to B and onto C. The outcome of this is the inevitable increase in repulsive forces between these cations, which will then be constrained to sites where their repulsions are minimum, i.e., centers of the octahedral sites in the previously described clusters. As stated earlier this is consistent with the decrease in T_C.

References

1. B. Elouadi, M. Zriouil, J. Ravez, and P. Hagenmuller, *Ferroelectrics* **38,** 793 (1981).
2. B. Elouadi, M. Zriouil, J. Ravez, and P. Hagenmuller, *Mater. Res. Bull.* **16,** 1099 (1981).
3. B. Elouadi, M. Zriouil, J. Ravez, and P. Hagenmuller, *Ferroelectrics* **56,** 21 (1984).
4. M. Zriouil, B. Elouadi, J. Ravez, and P. Hagenmuller, *J. Solid State Chem.* **51,** 53 (1984).
5. M. Zriouil, J. Senegas, B. Elouadi, and J. B. Goodenough, *Mater. Res. Bull.* **20,** 679 (1985).
6. M. Zriouil, these de DES de 3eme Cycle, Faculte des Science, Rabat, Morocco (1981).
7. B. Guenais, M. Baudet, M. Minier, and M. Le Cun, *Mater. Res. Bull.* **16,** 643 (1981).
8. T. P. Pearsall, S. Chiang, and R. V. Schmidt, *J. Appl. Phys.* **47,** 4794 (1976).
9. M. Fukuma, J. Noda, and H. Iwasaki, *J. Appl. Phys.* **49,** 3693 (1978).
10. M. Minakata, S. Saito, M. Shibata, and S. Miyazawa, *J. Appl. Phys.* **49,** 4677 (1978).
11. K. Sugii, M. Fukuma, and H. Iwasaki, *J. Mater. Sci.* **13,** 523 (1978).
12. M. Minakata, S. Saito, and M. Shibata, *J. Appl. Phys.* **50,** 3063 (1979).
13. W. K. Burns, P. H. Klein, E. J. West, and L. E. Plew, *J. Appl. Phys.* **50,** 6175 (1979).
14. S. Miyazawa, *J. Appl. Phys.* **50,** 4599 (1979).
15. J. Jackel, A. M. Glass, G. E. Peterson, C. E. Rice, D. H. Olson, and J. J. Veselka, *J. Appl. Phys.* **55,** 269 (1984).
16. R. D. Shannon and C. T. Prewitt, *Acta Crystallogr. Sect. B.* **25,** 925 (1969).
17. K. Nassau, H. J. Levinstein, and G. M. Loiacono, *J. Phys. Chem. Solids* **27,** 989 (1966).
18. S. C. Abrahams and E. T. Keve, *Ferroelectrics* **2,** 129 (1971).